β-Amyloid Targeting with Two-Dimensional Covalent Organic Frameworks: Multi-Scale In-Silico Dissection of Nano-Biointerface

Reza Maleki,[a] Mohammad Khedri,[b] Sima Rezvantalab,*[c] Fatemeh Afsharchi,[d] Kiyan Musaie,[d] Sepehr Shafiee,[e] and Mohammad-Ali Shahbazi*[d, f]

Cytotoxic aggregation of misfolded β-amyloid (Aβ) proteins is the main culprit suspected to be behind the development of Alzheimer's disease (AD). In this study, Aβ interactions with the novel two-dimensional (2D) covalent organic frameworks (COFs) as therapeutic options for avoiding β-amyloid aggregation have been investigated. The results from multi-scale atomistic simulations suggest that amine-functionalized COFs with a large surface area (more than 1000 m^2/gr) have the potential to prevent Aβ aggregation. Gibb's free energy analysis confirmed that COFs could prevent protofibril self-assembly in addition to inhibiting β-amyloid aggregation. Additionally, it was observed that the amine functional group and high contact area could improve the inhibitory effect of COFs on Aβ aggregation and enhance the diffusivity of COFs through the blood-brain barrier (BBB). In addition, microsecond coarse-grained (CG) simulations with three hundred amyloids reveal that the presence of COFs creates instability in the structure of amyloids and consequently prevents the fibrillation. These results suggest promising applications of engineered COFs in the treatment of AD and provide a new perspective on future experimental research.

Introduction

Alzheimer's disease (AD) is the most common neurodegenerative disorder in the world. millions of people worldwide are suffering from its disruptive consequences.[1,2] To date, there is no cure available for AD. Therapeutic management only includes controlling symptoms and neuropsychological signs with drugs that balance neurotransmitters alongside behavioral intervention and rehabilitation.[3,4] A leading hypothesis concerning the pathology behind AD is the aggregation of β-amyloid fibrils and abnormal β-amyloid depositions that can interfere with the neural function, resulting in the apoptosis of neurons.[5] In recent years, many efforts have been dedicated to a therapeutic solution for preventing β-amyloid aggregation.[6–9] These structures usually consist of misfolded β-amyloid monomers (Aβ), a polypeptide that consists of 34–43 amino acids with a dominant secondary structure of β-sheets.[10] The formation of β-amyloid fibril is considered a self-propagating process, as a misfolded β-amyloid monomer can induce conformational changes in other peptides and promote the formation of oligomers and, finally, β-amyloid fibrils. It is believed that Aβs are produced by the cleavage of β-amyloid precursor protein or β-amyloid precursor protein (APP) by enzymes like Meprin-β, and γ secretase.[11] APP can typically be found in the membrane of neurons, and it is considered a highly conservative type 1 single-pass transmembrane protein. However, its exact function is still unknown.[12,13] Although all forms of Aβ peptide seem to be cytotoxic, it has been suggested that Aβ peptide oligomers are more cytotoxic than any other form, including β-amyloid fibrils, and it can induce apoptosis by interfering with ion channels of neurons, which

[a] Dr. R. Maleki
    Computational Biology and Chemistry Group (CBCG)
    Universal Scientific Education and Research Network (USERN)
    19839-63113 Tehran (Iran)
[b] M. Khedri
    Computational Biology and Chemistry Group (CBCG)
    Universal Scientific Education and Research Network (USERN)
    19839-63113 Tehran (Iran)
[c] Dr. S. Rezvantalab
    Renewable Energies Department, Faculty of Chemical Engineering
    Urmia University of Technology,
    57166-419, Urmia (Iran)
    E-mail: srezvantalab@uut.ac.ir
[d] F. Afsharchi, K. Musaie, Dr. M.-A. Shahbazi
    Zanjan Pharmaceutical Nanotechnology Research Center (ZPNRC)
    Zanjan University of Medical Sciences,
    45139-56184 Zanjan (Iran)
    E-mail: m.a.shahbazi@helsinki.fi
[e] S. Shafiee
    School of Medicine,
    Shahid Beheshti University of Medical Sciences
    19839-63113 Tehran (Iran)
[f] Dr. M.-A. Shahbazi
    Drug Research Program
    Division of Pharmaceutical Chemistry and Technology
    Faculty of Pharmacy,
    University of Helsinki,
    00014 Helsinki (Finland)

    Supporting information for this article is available on the WWW under
    https://doi.org/10.1002/cbic.202100075

ChemBioChem

Full Papers
doi.org/10.1002/cbic.202100075

**Chemistry
Europe**
European Chemical
Societies Publishing

can result in an influx of calcium ions leading to inevitable cell death.[14,15]

Nanoparticles can affect the conformation and assembly of proteins by altering the number of hydrogen bonds, van der Waals (vdW), and electrostatic forces.[16–19] Many studies have been conducted on the potential use of nanoparticles in the treatment of neurodegenerative diseases caused by abnormal accumulation of β-amyloid s, such as AD, Parkinson's disease, and Huntington disease.[16,20,21] Although it has been shown that some nanoparticles can promote the aggregation of β-amyloids,[22] many other nanoparticles have shown promising results for preventing β-amyloid formation or dissolving β-amyloid fibrils.[23–28] For instance, Javed *et al.* demonstrated that casein-coated gold nanoparticles could inhibit the formation of Aβ structures in zebrafish.[29] In another study conducted by Giannousi *et al.*,[30] zinc-doped ferrite nanoparticles were used to interfere with the formation of Aβ structures.; *Liu et al.*[31] also observed the ability of graphene quantum dots to act as a regulator for the formation of β-amyloid fibrils.

Biocompatibility, pharmacokinetics, tunability, as well as the ability to prevent β-amyloid fibrillation can influence the selection of nanoparticles for AD treatment. Covalent organic frameworks (COF) are a new generation of nanoparticles with two or three-dimensional structures and strong bonds constructed from carbon, oxygen, nitrogen, and hydrogen atoms.[32,33] These nanoparticles are one of the most highly tunable nanoparticles that have also shown high biocompatibility and great potential for application in biomedicine,[34–38] as well as drug delivery[39] and cancer therapy.[36,40] Because of their high tunability, the structure of COF can be designed for different purposes, such as enhancing diffusion through the blood-brain barrier or preventing β-amyloid aggregation. Meanwhile, with recent advances in computer sciences, molecular dynamics are becoming a valuable tool for designing new drugs to provide insight into molecular system interactions (*e.g.*, β-amyloid aggregation, drug delivery, protein-protein interactions, etc.). For instance, in a combinational study by Ciudad *et al.*,[41] the MD simulation together with nuclear magnetic resonance (NMR) and mass spectrometry (MS) provided pieces of evidence on the mechanism for the neurotoxicity of Aβ as the leading cause of AD. Such simulations can be beneficial for narrowing down the potential agents that can be used for AD treatment.[31,42–48]

In this study, for the first time, the potential utilization of new generations of 2D-COFs in preventing β-amyloid aggregation was investigated by analyzing their interactions with Aβ amyloids using a multi-scale computational approach. COFs are biocompatible nanomaterials that can be tailored and customized for diverse settings and applications, making them favorable materials to work with. As a second novelty, we have employed surface chemistry engineering and morphology studies to create a variety of COFs and subsequently measure parameters to evaluate the effectiveness of each monolayer in preventing β-amyloid aggregation. After the in-silico study of COF effects on β-amyloid aggregation, their impact on β-amyloid fibrillation was studied using molecular simulations and umbrella sampling. A significant factor for potential drugs

is the ability to reach their specific target tissue, in this case, the brain. Ergo we used a molecular dynamics simulation approach to assess the penetration of the COFs through the BBB membrane. All molecular simulation methods were validated using experimental and computational references.

To overcome the shortcomings of the all-atom method, coarse-grained (CG) simulations have been performed with a higher number of β-amyloid and COFs. This method has been used to validate the results on a larger scale. On account of the fact that each simulation approach has its share of limitations, we have adopted a multi-scale approach to this problem. Altogether, the results pave a new way for researchers to investigate the potential application of COFs in the inhibition of AD disease.
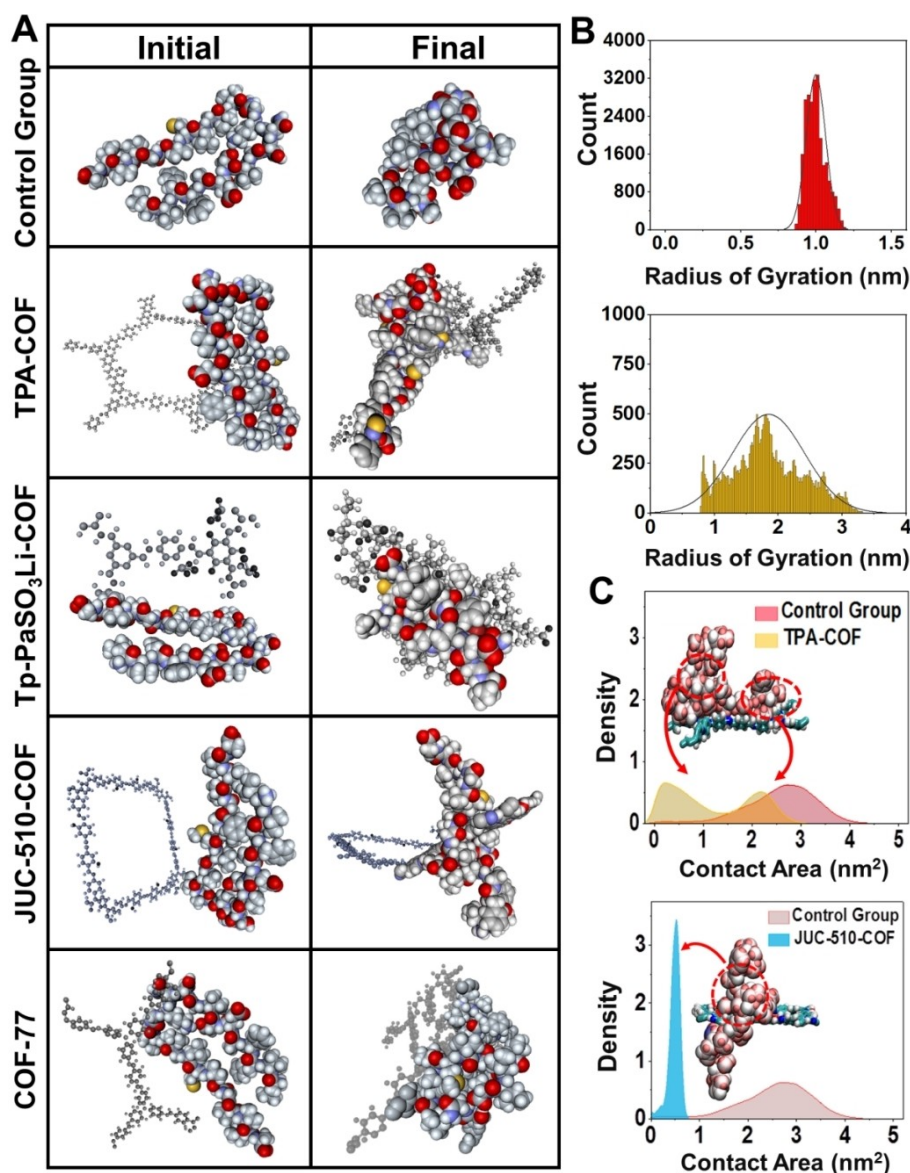
Results and Discussion

Fundamental assessments

The formation of fibril plaques is a complex process due to the formation of oligomers, protofibrils, and finally, mature fibrils.[49,50] The formation of a compact nucleus is an essential step for the aggregation process of Aβ and the development of β-amyloid fibrils. Figures S1A and B and Table S1 show the structures of Aβ monomer and COF-compounds used in the simulations, respectively.

Three related references were used to validate the simulation method of this work. One of the references included *in vivo* test and two of them involved molecular simulation works. The method and conditions of all 3 references were simulated using our method, and the results are compared with the results of the references. Figure S2 presents the comparison of repeated simulations with references. These results confirm the precision of the algorithms and the simulation methods of the current study.

Snapshots are provided in Figures 1A and S3.A at the initial (0 ns) and the final stage (50 ns) of the simulation to deliver a visual perception of the study. First, to assess the stability of the molecular systems, the root mean square deviations (RMSD) as criteria of the system's stability has been analyzed.[51,52] RMSD evaluates the average distance of atoms and their fluctuations in organic molecular systems (Figure S3.B). The plot shows that utilizing TPA-COF alters the range of fluctuations for the β-amyloid monomer. In other words, for all simulations, after almost 20 ns, RMSD diagrams fluctuate within a 0.2 nm region. For instance, although the COF-77 corresponding line has elevated RMSD values in the initial stages of simulation, after almost 10 ns it fluctuates within a small range. While for the TPA-COF case, not only the range of oscillations is more than 2.5 nm but also, towards the end of the simulation, it drops to lower values compared to the initial stages. The observed results can be attributed to the higher interactions of the β-amyloid monomer with TPA-COF nanomaterial.

Another similar evaluation known as mean square fluctuation (RMSF) indicates the stability of a molecular system by calculating an atom's deviations from its position in a specific

ChemBioChem

Full Papers
doi.org/10.1002/cbic.202100075

Chemistry
Europe
European Chemical
Societies Publishing

Figure 1. Aggregation of Aβ in the presence of COF compounds. A) Initial structure and final assembly of Aβ monomer that is introduced into the simulations without and with COF structures (as TPA–COF, Tp–PaSO₃Li–COF, JUC–510–COF, and COF–77). B) Rg distribution for Aβ during the bare simulation and in the presence of TPA–COF. Broadened Rg distribution is indicative of prohibited aggregation, while a narrow gyration radii distribution represents a compact aggregate. C) Comparison of the contact area of β-amyloid monomers as the control group with the monomers under the attack of TPA–COF and JUC–510–COF, respectively.

period. Higher fluctuations in RMSF diagrams indicate the instability of a molecular system. Higher RMSF values represent more exposure to the solvent;[53] therefore, nanoparticles that induce greater changes in these values can prevent Aβ aggregation. Figure S3.C reveals RMSF values as a function of atom in the presence of COF-nanomaterials. The control group is the simulation of β-amyloid fibrillation without the presence of COF-compounds to precisely monitor and compare the effect of COF compounds. The simulation clearly shows the higher RMSF values that can be observed in the presence of TPA-COF, JUC-510-COF in comparison with the reference simulation. As noted, these nanomaterials can interact with the Aβ monomer to inhibit fibril formation. Interestingly, the CH₃-Li–ImCOF

compound shrinks the RMSF ranges, which indicates its ability to enhance the peptide aggregation.

The formation of a compact nucleus is an essential step for the aggregation of Aβ and the development of β-amyloid fibrils. In this regard, the radius of gyration (Rg) can be used for assessing the compactness of the molecular structure. A decrease in the values and lesser variation of Rg can be interpreted as the structure aggregates and becomes more compact. As is well-known, during the simulation, gyration radii vary with time. However, to better and quantitatively evaluate its variations, Rg distributions are investigated in each case. Figure 1B shows two samples to exhibit the effect of COF in the Rg distribution for TPA-COF and Tp-PaSO₃Li-COF, respectively.

ChemBioChem

Full Papers
doi.org/10.1002/cbic.202100075

Chemistry Europe
European Chemical
Societies Publishing

Table 1. The aspect ratio of COFs and simulation results with and without the structures.

Monolayer	Control	TPA—COF	Tp—PaSO₃Li—COF	CH₃>Li—ImCOF	COF—OEt	JUC—510—COF	COF-77
Contact area (nm²)	1.0896	0.7069	1.5703	0.8634	1.6283	0.4917	2.0305
Aspect ratio of COF	–	1.1	2.1	1.9	1.3	1.0	1.5
Average number of H-bonds	61.681 ± 5.486	66.518 ± 6.145	62.545 ± 5.683	61.557 ± 5.227	65.461 ± 4.776	68.644 ± 5.266	64.763 ± 6.19033

The inhibition of Aβ monomer aggregation is evident from the obvious broadened distribution of Rg with TPA COF. Inspected with more detail, it can be noticed that TPA-COF causes an extended Rg distribution from less than 1 nm to more than 3 nm. However, the extension range of Rg for JUC-510-COF and COF-OEt is between 1 to 1.5 nm, which reveals a lower inhibition ability of the sample against the aggregation. In other words, with the presence of TPA-COF, JUC-510-COF, and COF-OEt, the Rg increases, which points to the fact that the presence of these nanoparticles could reduce the compactness of Aβ and prevent β-amyloid aggregation. However, the existence of Tp-PaSO₃Li-COF promotes the formation of a packed structure with a single peak of Rg distribution at less than 1 nm, which is even less than the initial Rg. Moreover, the presence of CH₃—Li—ImCOF also enhances β-amyloid aggregation since it induces more compact conformations in Aβ protein. For the continuance/extension β-amyloid aggregation, its' monomers need to interact so that the misfolded proteins induce β-amyloid-forming conformations in other β-amyloid monomers.
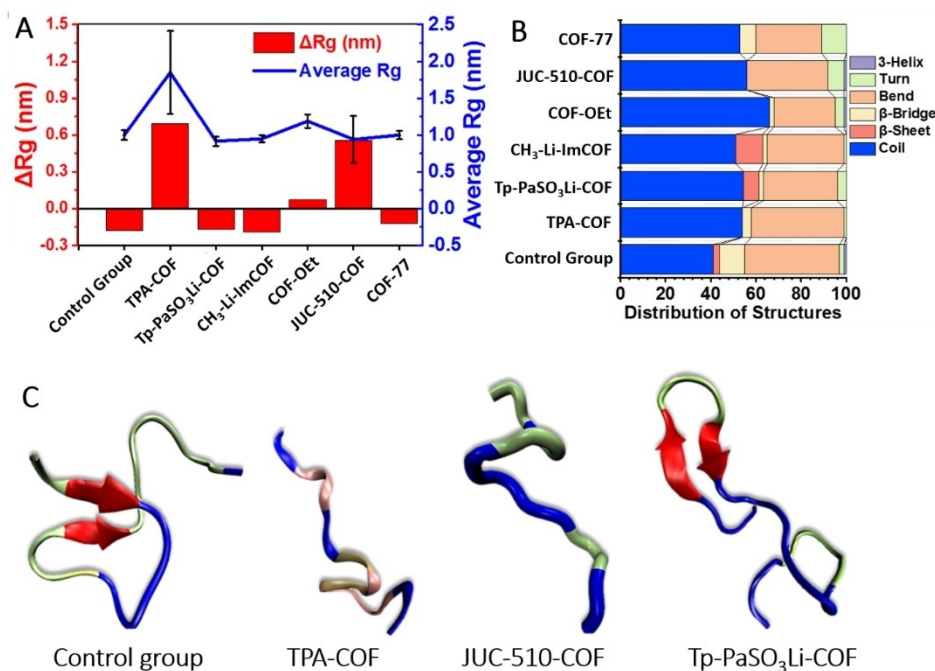
To assess the contact area of protein, solvent-accessible surface area analysis, or SASA can be used.[54–56] Herein, SASA analysis was used for investigating the contact area of Aβ in the presence of COFs. The lowest average contact areas were seen in the presence of JUC-510-COF and TPA-COF, closely followed by CH₃—Li—ImCOF (Table 1). Figure 1C shows the average contact area of the Aβ monomers for three simulations with JUC-510-COF, TPA-COF, and Tp-PaSO₃Li-COF in addition to the molecules snapshots to provide better insight into the data. Surprisingly, despite the lowest contact area of Aβ in the existence of JUC-510-COF, the most favorable results considering the avoidance of polypeptide molecule self-assembly is found with the accompaniment of TPA COF. The perceived results can be attributed to the aspect ratio of the COFs. In other words, symmetrical structures with an aspect ratio of one provide more surface for Aβ. Table 1 shows the aspect ratio of considered COF-compounds. It can be seen that the aspect ratio of 1 and 1.1 offer a better available surface area for β-amyloid and reduce the contact area of the β-amyloid strands with itself. Moreover, it can be seen that during the simulation, half of the TPA-COF arms bend back (Figure 1C) and offer no contact area for the Aβ molecule, which results in a boost in the self-contact area for the biological molecule. In conclusion, the aspect ratio and morphology must be taken into account as an effective factor in the interactions. Figure 2A outlines the average Rg throughout the simulation in addition to the ΔRg, which represents the difference between final and initial gyration radii. As can be seen, Aβ monomers enlarge in the case of TPA—COF, JUC—510—COF, and COF—OEt, where the ΔRg values are positive. The average of Rg of Aβ is ∼1 nm, while Tp-

PaSO₃Li—COF, CH₃—Li—ImCOF promote tighter fibril aggregates. However, the presence of these compounds resulted in a more compact conformation of Aβ protein, which means that these specific COFs can induce β-amyloid fibrillation.

The type and number of secondary structures such as β-sheets, α-helix, turns, and coils can determine the fate of the final conformation of proteins due to the fact that α-helix to β-sheet transition is considered the first stage of β-amyloid aggregation.[57] Evaluating this local folding can predict the ability of Aβ polypeptides to form β-amyloid fibrils. As mentioned before, β-amyloids have a high amount of β-sheet structure, and amyloid aggregates can induce these motifs in an unfolded Aβ polypeptide. β-sheets have been strengthened by H-bonds between amino acids of the polypeptide chain and make the backbone of β-amyloid fibrils. For an intensive analysis of the ability of Aβ monomer to induce amyloid conformations in other proteins, the secondary structures of amyloid protein in the nanoparticles' presence has been assessed (Figure 2B). As is apparent in this figure, the presence of CH₃—Li—ImCOF and Tp—PaSO₃Li—COF induce β-amyloid conformations with higher amount β-sheets in comparison with the control group, while the presence of COF—OEt, JUC—510—COF, and TPA—COF reduce the number of β-sheets in β-amyloid to zero percent. The observation of the distributed H-bonds on the overall structure of a β-amyloid molecule with water leads to the presence of loose coil- and bend-rich conformations. In contrast, it can be noticed that CH₃—Li—ImCOF and Tp—PaSO₃Li—COF enhance β-sheet percentage in the average conformations and lead to boosted β-amyloid aggregations. Figure 2C displays examples out of all simulation cases that form various conformations under the COF attack. The denser β-sheets for the Tp—PaSO₃Li—COF case are easily noticeable, which is proof of its unfavorable impact, *i.e.*, it can trigger assembly of the polypeptide. On the other hand, scattered β-amyloid monomers accompanied by the TPA—COF and JUC—510—COF nano-objects proves that their presence is advantageous.

In this context, to obtain in-depth information about Aβ and COF interactions, a quantitative measure of charge distributed over the Aβ structure was acquired. As is known, Aβ consists of a plural number of varying amino acids. Figure S4 represents the polypeptide used in the current study. Figure 3A exhibits the functional groups of residues with a scale of charge that can impact the Aβ interactions, conformation, and final state. As shown there, the charge of residues can vary from −1 for GLU and ASP containing carboxylate groups to +1 for LEU and LYS components of amine groups. Next, the surface charge of COF compounds and β-amyloid monomer (Figures 3B1 and S5) were characterized. Similar to previous sections, only the
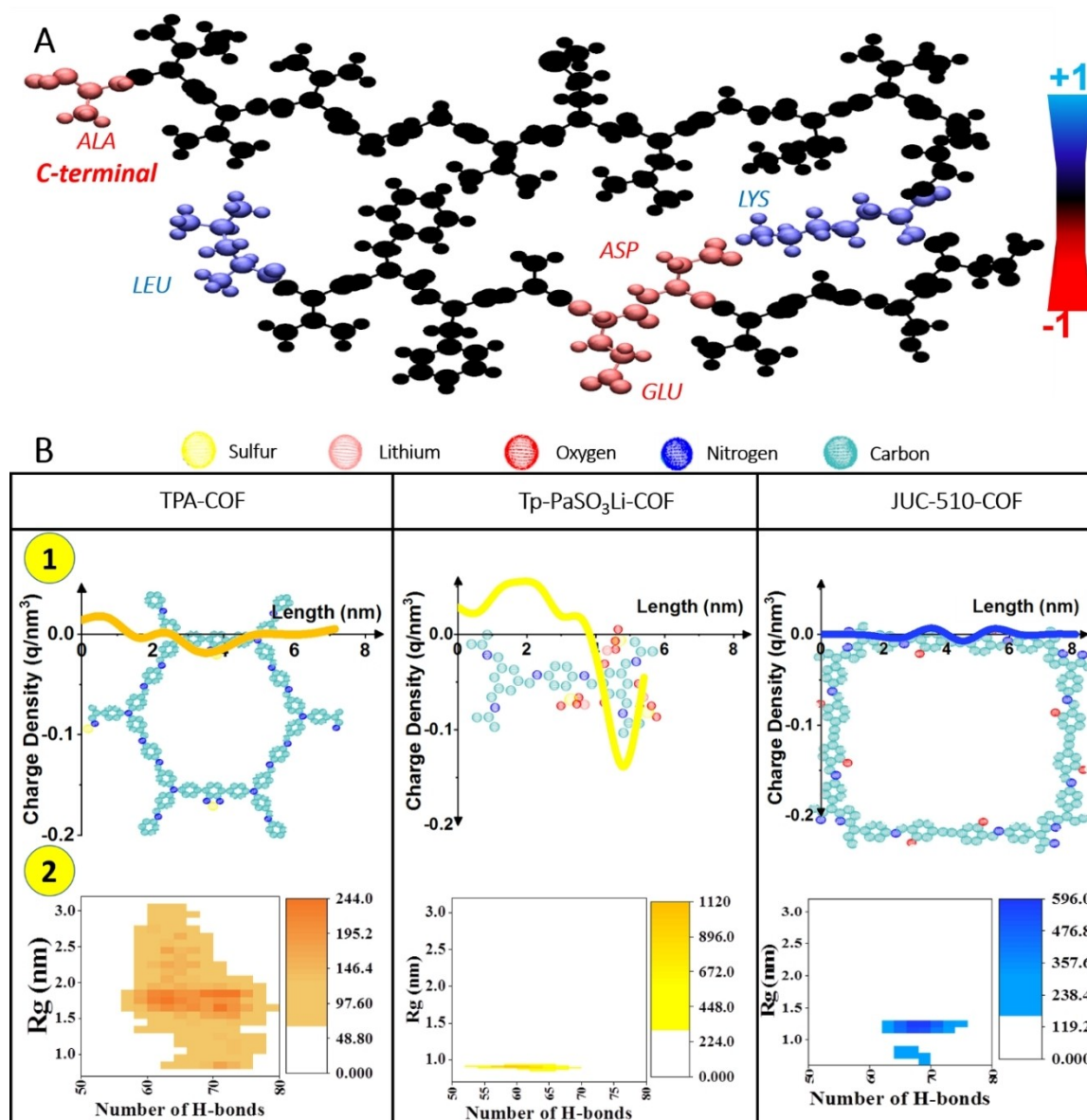
ChemBioChem

Full Papers
doi.org/10.1002/cbic.202100075

Chemistry
Europe
European Chemical
Societies Publishing

Figure 2. A) The average Rg and ΔRg (as the difference between final and initial Rg values) both illustrate that TPA–COF, JUC–510–COF, and COF–OEt extend the Aβ monomer and avert its aggregation. B) Distribution of secondary structures of β-amyloid during the simulations. The accompaniment of TPA–COF, JUC–510–COF, and COF–OEt decreases the β-sheets to zero and promotes the coil and bend conformations in the structure. While the presence of PaSO₃Li–COF enhances β-sheets compared to the control group. C) Snapshots of Aβ strands at the end of simulation validate the quantitative observations of structural conformations observed in the distribution of secondary structure plot.

charge distributions of TPA–COF, Tp–PaSO$_3$Li–COF, and JUC–510–COF were exemplified since they have highlighted behavior. The most striking observation is that the Tp-PaSO$_3$Li-COF with the most negative and positive charge distribution (overall neutral charge) on the surface has, in fact, an unfavorable effect on the Aβ monomer, where it promoted the formation of the more compact assembly compared to the reference model. The Tp–PaSO$_3$Li–COF structure contains three Li atoms (positively charged) together with 12 oxygen atoms that are responsible for the overall negative charge. It is clear (Figure 3B1) that in the region with a higher density of oxygen, the overall charge drops to particularly negative values. Shockingly, residues of β-amyloid interacted weakly (Figure S5) with CH$_3$–Li–ImCOF with a positive region on the charge distribution plot (but overall neutral structure), i.e.. the COF can promote conformational changes in the structure of Aβ monomer that can eventually lead to the formation of β-amyloid fibrils.

The number of hydrogen bonds (H-bonds) is one of the most critical factors determining the final state and conformation of polypeptides. A high number of hydrogen bonds between water molecules and proteins can increase the solubility of the protein. In the case of Aβ, an increase in the number of hydrogen bonds with water can result in the impeded β-amyloid aggregation. H-bonds, a type of interaction with adjacent water molecules, significantly affect the secondary structures of the proteins. An increase in the number of β-sheets and a decrease in the number of turns and coils are in favor of conformations with an ability to develop β-amyloid fibrils. In other words, an increased number of H-bonds with water manifest coil-rich conformations of β-amyloid that can hinder β-sheets formations.[49] To better understand the effect of H-bonds with adjacent water molecules on the structural deformation of Aβ monomer, gyration radii as a function of H-bond number (Figure 3B2 and Figure S5) has been plotted. According to Baumketner,[58] a high number of H-bonds in the minima corresponds to aggregated states, which can be seen in the case of Tp–PaSO$_3$Li–COF compared to the control group. For instance, the main region is centered at (Rg; H-bond number) value of (0.91 nm; 1119) for Tp–PaSO$_3$Li–COF. The minima for the control group and TPA–COF are located at (0.93 nm; 546) and (1.7, 1.8 nm; 240, 240). A lower number of H-bonds with expanded values of Rg points out to the hindered aggregation.[49] On the other side, lower Rg values with a higher number of H-bonds (with Tp–PaSO$_3$Li–COF) can be a sign of a region with higher β-sheet content.[58]

Table 1 presents the average number of H-bonds for Aβ-water interaction in the course of the simulation, which confirms higher hydrophilicity. Despite the observed maximum H-bond at minimum Rg for Tp–PaSO$_3$Li–COF, the highest average amount of hydrogen bonds was observed in the presence of JUC–510–COF and TPA–COF. As it is clear, a higher average number of H-bonds with water extends Aβ in a higher range of Rg, i.e., it prevents the aggregation of Aβ. Furthermore, it was observed that the presence of CH$_3$–Li–ImCOF could reduce the mean number of hydrogen bonds. Figure 4A shows

ChemBioChem

Full Papers
doi.org/10.1002/cbic.202100075

Chemistry
Europe

European Chemical
Societies Publishing

Figure 3. A) Effective functional groups in the structure of the Aβ monomer. B1) Charge distribution on the surface of 2D COFs: TPA–COF, Tp–PaSO₃Li–COF, and JUC–510–COF, respectively. It can be understood that the highly negative surface of COFs, leads to promoted aggregation of Aβ monomer. B2) Rg map showed as a function of H-bonds with surrounding water molecules for the control group, with TPA–COF, Tp–PaSO₃Li–COF, and JUC–510–COF. This method can be used as an illustration of molecule conformation. Consistent with previous results, extended Aβ monomer forms H-bonds with neighboring water molecules on its structure.

snapshots of the Aβ monomer scattered towards the water molecules that verify the amplified interactions with water when accompanied by COF. Solvent accessible surface area (SASA) is extracted to examine the hydrophobic and hydrophilic surface areas that can induce conformational changes.

Furthermore, the anti-β-amyloidogenic ability of the COF-compounds can be investigated from an energetic point of view. To date, many studies have been published on the control of other properties such as hydrophobicity of agents[53,59] or π-stacking interactions[60] as the key point of inhibitory effect. Results of another study conducted by Baweja *et al.* in which interactions between Aβ and graphene oxide suggested that

nanoparticles can inhibit the formation of β-amyloid by reducing the number of β-sheets through hydrophobic interactions.[53] This study concluded that β-amyloid fibrillation was inhibited through strong hydrophobic interactions between Aβ and Fullerene and the consequent prevention of β-sheet formation. Furthermore, Li *et al.*[61] observed that in the simulation of Aβ with a single-walled carbon nanotube, weak hydrophilic interactions were capable of inducing conformations in Aβ that d promotes β-amyloid aggregation. On the other hand, due to the fact that electrostatic interactions between nanomaterials and peptides can play a determinant role in the disaggregation of the biological components, the
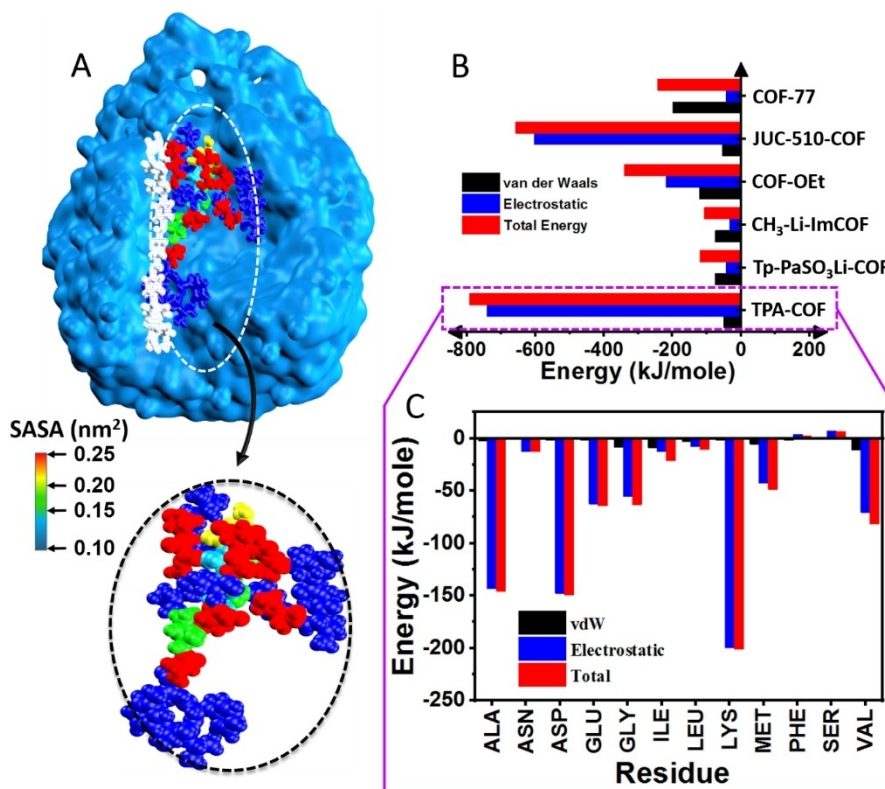
Figure 4. A) Snapshots of Aβ as interacting with surrounding water molecules. The extension of Aβ molecules in the presence of COF molecules promotes its solubility and avoid its precipitation. B) Average interaction energy of polypeptide and an organic compound, including vdW, electrostatic, and total energy interactions. C) The evaluation of the individual residues interactions with TPA–COF.

electrical field has been considered as an unfolding factor for β-amyloids.[58,62,63] For instance, recently, Saikia *et al.*[64] experimentally observed that low-strength electric fields can impede the self-assembly of short peptides. In this line, the interactions between β-amyloid monomer and the COFs mainly consisted of non-bonded interactions, *e.g.*, vdW, electrostatic, and hydrophobic interactions were assessed. To provide a clear view of the interactions, the mean values of interaction energies are plotted in Figure 4B. Regarding the figure, Aβ has the highest affinity towards TPA-COF among its peers, which is mainly driven by electrostatic attractions. It is noted that electrostatic bonds are the main molecular interaction for TPA–COF and JUC–510–COF, which have favorable effects on the prevention of fibril formations. A high absolute amount of energy is an indicator of strong interactions between nanoparticles and Aβ monomers. Although the vdW energy played an important role in the interaction of CH₃–Li–ImCOF and Tp–PaSO₃Li–COF with Aβ, it was not sufficient enough to provide significant results in impeding fibril formations. It is worth pointing out that electrostatic interactions were found as the interfering force in the fibrillation process of β-amyloid s using graphene nanosheets, carbon nanomaterials, etc.[53,65,66] According to Figure 4A, our results also confirm that in any successful interaction between nanomaterial and Aβ, the electrostatic interaction energy is the driving force. Although both electrostatic and vdW forces contributed to total energy interaction between all COFs and

Aβ, it was observed that the role of electrostatic interactions was more prominent than vdW forces in JUC–510–COF/Aβ and TPA-COF/Aβ interactions. In contrast, vdW forces played a more notable role in Tp–PaSO₃Li–COF and CH₃–Li–ImCOF interactions with Aβ. This can indicate that the surface charge of interacting structures (both Aβ and COFs) have a crucial role in the self-assembly of Aβ.

To scrutinize the binding of Aβ and COFs, energy analysis for individual residues was performed (Figures 4C and S6) in each simulation. The most contributing residues can be identified for simulations with TPA–COF using Figure 4C. For instance, LYS has the most contribution to the overall interactions through electrostatic energy for the successful inhibition of self-assembly, using TPA–COF. During this study, it was noticeable that changes in the aspect of the COF compound that all had neutral charge can trigger the formation of an β-amyloid monomer, which can be considered as the start of the fibrillation process. Strong affinity and binding of Aβ strands are observed in the neutral COF compounds with an aspect ratio rather close to one. Moreover, it was concluded that due to the varying charge of residues present in the β-amyloid structure, manipulation of COF surface charge density could result in better outcomes. To address these important points, in the following sections, we investigated the effect of charge and morphology of COFs in more detail.

ChemBioChem

Full Papers
doi.org/10.1002/cbic.202100075

**Chemistry
Europe**
European Chemical
Societies Publishing

Physicochemical properties of COFs in the interaction with β-amyloid

According to Mohammad-beigi *et al.*,[67] charged nanoparticles significantly can shift their interaction with biological molecules. It can be understood that surface charge and aspect ratio can change their performance in attacking β-amyloid. As mentioned earlier, the morphology of the COF molecules could affect their interactions with β-amyloid fibrils. Figure 5A exhibits the three COF compounds from the first part that showed promising results, with shifted aspect ratios. To add rigor to our

hypothesis, COFs with the same molecular composition but different aspect ratios were designed. Additionally, to reveal the charge effect of COFs, only three successful COFs (TPA–COF, JUC–510–COF, and COF–OEt) were considered (Figure 5B). To this end, COFs–NH$_2$ (COF+) and COFs–COOH (COF−) are introduced to the simulation box to monitor their interaction with β-amyloid monomers. To demonstrate the important role of the surface charge of COFs, the interactions of individual residues corresponding to charged nano-objects are evaluated. Similar analyses are conducted for the rest of the COFs considered in the previous part (Figures S7 and S8, and
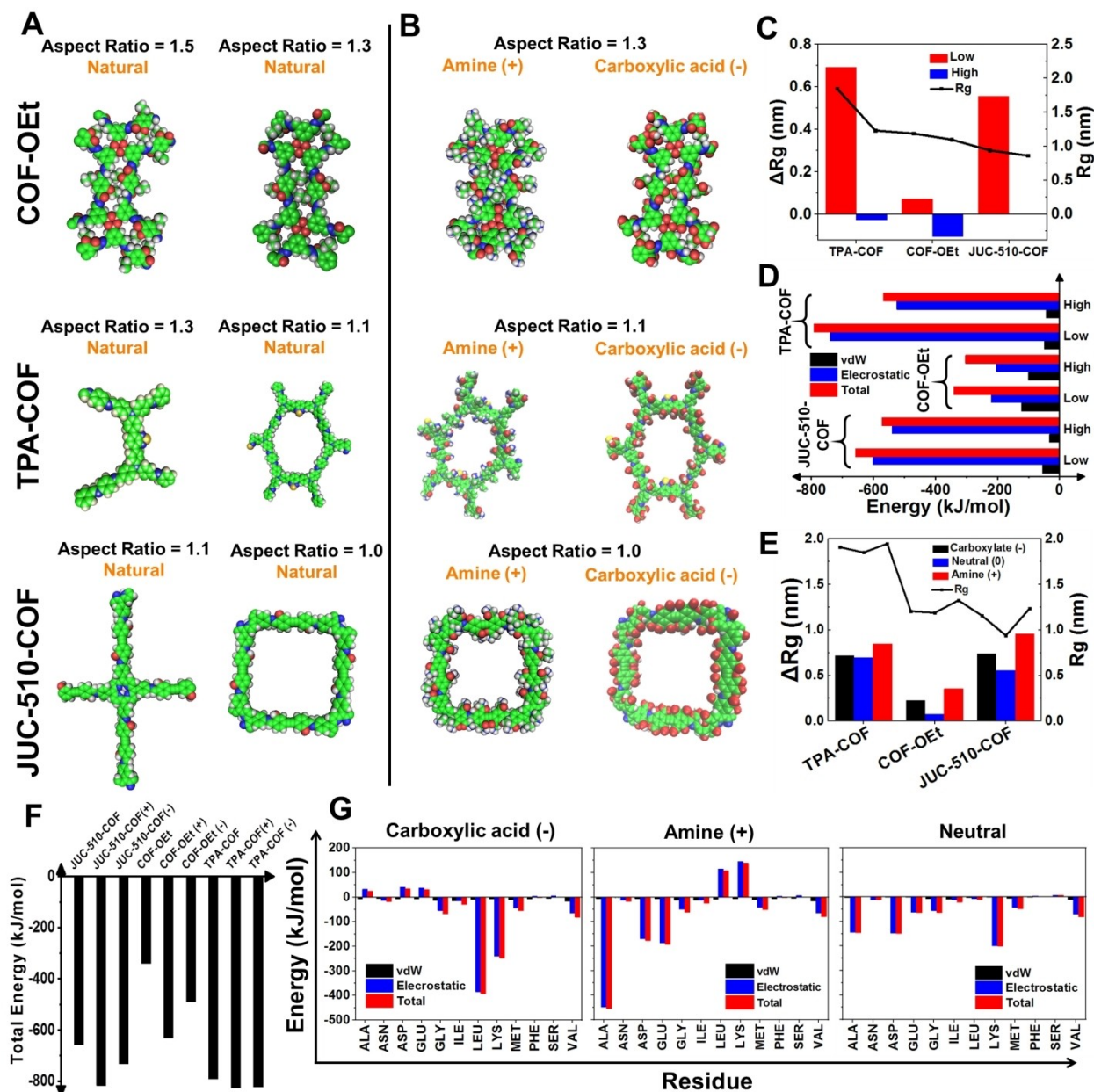
Figure 5. Investigation of the physicochemical properties of the COF molecules in the interaction with amyloid. A) the molecular structure of an organic compound with the same number of atoms and compositions but different aspect ratio. B) Graphical representation of COFs with negative and positive charges. C) ΔRg and average Rg size plotted vs. morphological change. D) Interaction energies as a function of molecular design show the impact of aspect ratio. E) Rg and ΔRg for COFs with varying surface charges that clearly show COFs(+) extend β-amyloid molecules when exposed to. F) Binding energies of three COFs with varying functional groups on the surface. G) Detailed analysis of β-amyloid residues with charged JUC–510–COF.

ChemBioChem   Full Papers
doi.org/10.1002/cbic.202100075

Chemistry
Europe
European Chemical
Societies Publishing

Table S2). As can be seen in Figure 5C and D, a simple change in the molecule geometry can influence the aspect ratio. This is achievable in the laboratory due to the highly tunable morphology of COFs. The systematic analysis of the β-amyloid adsorption to COF by increasing aspect ratio and keeping constant composition shows that in all cases, a lower aspect ratio (close to one) interfere with the aggregation of Aβ strands. In more detail, a small increase in the aspect ratio in each case has a significant impact on the ΔRg ($Rg_{final}-Rg_{initial}$). For instance, for COF–OEt with an alteration of the aspect ratio from 1.0 to 1.1, ΔRg is shifted from $+0.07$ to -0.1, *i.e.*, the β-amyloid molecule formed a compact assembly compared to its initial state. A similar trend has been observed for all COFs where organic compounds with a higher aspect ratio assisted the formation of tighter β-amyloid aggregates. Similar behavior was observable for energy analysis were compared with lower aspect ratio, COFs with higher aspect ratio have lower energy interactions with biologic molecule demonstrating reduced capability in attacking the molecule. Part I of Table 2 displays more consequences of change in the organic molecules' morphology. In other words, H-bonds with adjacent water molecules and DSSP instability drops, while the self-contact area of Aβ and its stability increases with a higher aspect ratio . these are all unfavorable results.

For all cases, average Rg and ΔRg are increased in the interaction with positive surface charged nano-objects (Figure 5E). COFs with carboxylate functional groups (negative charge) offer better results compared with neutral surfaces. Similar results are observable for energy analysis (Figure 4F) where COF-compounds with positive charge performed better than the negative surface which itself acted better than neutral surfaces. These outcomes can be attributed to the β-amyloid structure with overall negative charge density that can interact better through the attractions with positive groups. The related results are summarized in part II in Table 2, where it is evident that the minimum self-contact area of Aβ is observed in COF(+) followed by COF(−) and finally COF(0). These results are consistent with Mohammad-Beigi *et al.*[67] results that the Aβ strand has a higher affinity toward charged nanoparticles rather than their neutral peers. Moreover, COF(+) accomplished the disaggregation better than COF(−) samples, which can be

attributed to the overall negative charge of the Aβ strand that causes stronger attraction between the biological molecule and COF-amine. In line with these results, a higher number of H-bonds with water molecules and higher instability of Aβ strands verifies the better performances of charged COFs, specifically COFs(+).
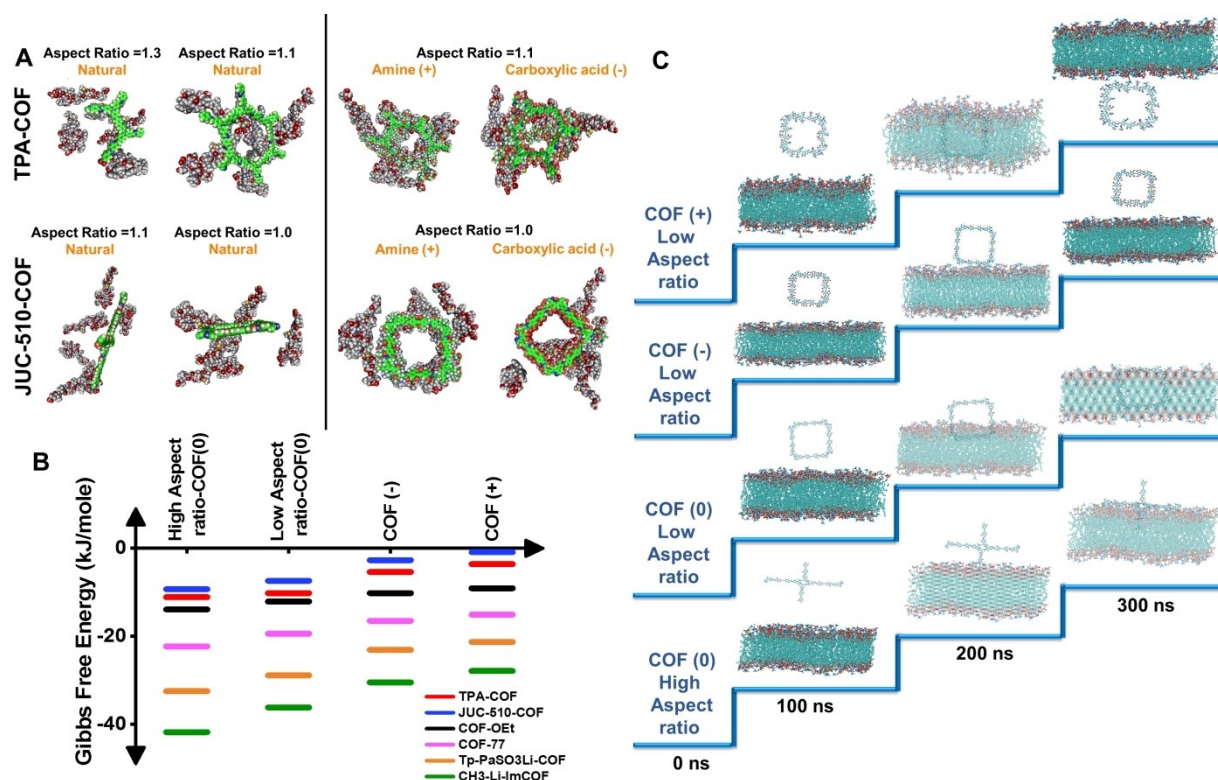
For all cases, average Rg and ΔRg also increase in the interaction with positive surface charged nano-objects (Figure 5E). COFs with carboxylate functional groups (negative charge) offer better results compared to neutral surfaces. Similar results were observed for energy analysis (Figure 5F). Figure 5G (and S8) highlights the binding of β-amyloid and JUC-510-COF (and COF-OEt and COF-TPA) with negative, neutral, and positive surface charge through its residues. As expected, residue energy analysis clearly shows that ALA, ASP, and GLUs (with negative charges) interaction are empowered with COFs (+). On the other side, LEU and LYS (with positive functional groups) are contributed to the energy magnitudes with COF(−). Interaction of neutral residues such as MET is unaffected with charge manipulations, which confirms the obtained results.

Inhibition of Aβ fibrillation by COF monolayers

As mentioned earlier, it has been proposed that Aβ oligomers or the most cytotoxic form of β-amyloids. Inspired by the findings of the previous simulations of this study, the simulations were extended to pentameric Aβ protofibril and their conformational changes in the presence of COF compounds. The results suggested that COFs can interrupt the protofibrilation stage in AD. Figures 6A and S9 illustrate the simulations and the outcomes for Gibbs free energy computations. Lower Gibbs free energy is indicative of a stable state that is an unwanted result in the inhibition of AD. In other words, any compound that can interrupt the formation of a stable Aβ protofibril can be designated as a successful agent to be utilized in further evaluations. Figure 6B shows the energy details of aggregations with considered COFs and their derivatives (with variable properties). It is noteworthy that the same calculations for the control group (pentameric Aβ protofibril) have revealed that change in the Gibbs free energy

Table 2. Comparison of COF performance with manipulated properties.

Effect of aspect ratio with engineered structures						
	TPA–COF		COF–OEt		JUC–510–COF	
Aspect ratio	1.1	1.3	1.3	1.5	1.0	1.1
Self-contact area of Aβ (nm^2)	0.52	0.84	1.967	2.218	0.49	0.53
Average number of H-bonds	66.52	65.26	65.46	65.02	68.64	66.32
Instability DSSP (turn + bend + coil)	0.96	0.95	0.97	0.95	0.99	0.96
Stability DSSP (3-Helix + 5helix + B-sheet + A-helix)	0	0	0.01	0.01	0.01	0.01

Effect of surface charge on COF performance									
	TPA–COF			COF–OEt			JUC–510–COF		
COF	(+)	(0)	(−)	(+)	(0)	(−)	(+)	(0)	(−)
Self-contact area of Aβ (nm^2)	0.45	0.57	0.50	1.25	1.97	1.649	0.39	0.49	0.43
Average number of H-bonds	75.50	66.52	69.98	66.94	65.46	66.28	77.98	68.64	70.25
DSSP (Turn + bend + coil) instability %	99	96	97	98	97	97	99	99	99
DSSP (3-helix + 5helix + B-sheet + A-helix) stability %	2	0	1	1	1	1	0	1	0

ChemBioChem

Full Papers
doi.org/10.1002/cbic.202100075

**Chemistry
Europe**
European Chemical
Societies Publishing

Figure 6. Gibbs free energy calculations for pentameric protofibril aggregations in the presence of COFs with varying properties. A) Snapshots of simulations of aspect ratios (low and high) and charge (negative, neutral, and positive) nanoparticles with Aβ pentamers. B) results from the computations reveal the relative stability of the Aβ pentamers with organic structures. C) Molecular simulation of crossing JUC—510—COFs through the BBB membrane at the different surface charge and functional group.

during precipitation is almost −46.4 kJ/mole, which is the lowest energy level among all cases. These results are aligned with previous parts of the current paper. It can be noticed that all COFs with lower aspect ratios have higher Gibbs energy levels, which are in correlation with Rg, enthalpy, and H-bonds results. Moreover, positively charge nano-objects have higher Gibbs free energy levels among their peers. The highest Gibbs free energy representative of prohibited aggregation is observed for CH₃–Li–ImCOF with positive surface charge and one aspect ratio.

COFs penetration through BBB

To prevent the harmful effect of β-amyloid deposition in the hippocampus and entorhinal cortex in ADs, clearance and reduction of the β-amyloid load from brain is proven to be effective.[68] Penetration through the blood-brain barrier (BBB) is one of the three pathways for the clearance of the β-amyloid.[68–70] Recently, the efflux of β-amyloid through the BBB have been studied in vitro and have shown it can be an effective approach in the ADs therapy.[71,72] The penetrating BBB, an endothelial cell network with highly selective permeability has remained a huge obstacle for designing pharmaceutical agents. Although many pharmaceutical agents have been investigated for their ability to prevent β-amyloid aggregation

due to their inability to diffuse into brain tissue, their potential application in ADs treatment has been limited. Therefore, for further investigation on the possible use of COFs and overcoming this obstacle, the interaction of COF nanoparticles with the BBB was simulated. According to references, the BBB membrane is the most important barrier for nanoparticles to cross for tissue targeting and drug delivery purposes. To investigate the effect of surface charge and aspect ratio, the penetration of COF nanoparticles with different functional groups and sizes of the BBB membrane was simulated. The BBB charge is considered to be negative due to the presence of glycosaminoglycan molecules on both the glycocalyx layer of the luminal side of endothelial cells and in the underlying basement membrane. Interestingly, due to the negative charge of the BBB membrane, COFs that are functionalized with the amine group (positive charge) pass better than the BBB membrane. As the results of our other analysis suggested that amine functional groups could improve COF function in preventing β-amyloid aggregation, the results of this simulation will further solidify their importance in preventing β-amyloid aggregation. Thus, the amine functional group improves the effect of COF in preventing the Aβ-amyloid aggregation as well as enhancing the COFs delivery across the BBB membrane.

Figure 6C outlines the molecular simulation of JUC-510-COF in different aspect ratios and with different functional groups. As shown in the figure, COFs, due to their hydrophobicity, tend

ChemBioChem

Full Papers
doi.org/10.1002/cbic.202100075

Chemistry Europe
European Chemical
Societies Publishing

to penetrate the BBB membrane, but their penetration over time is a function of the type of functional group and aspect ratio. The lower the aspect ratio, the greater the penetration of nanoparticles into the BBB membrane. This can be attributed to the higher contact area of the nanoparticles with the BBB in the low aspect ratio. The higher the contact area, the better the attraction due to hydrophobic, vdW, and electrostatic forces that can absorb adjacent molecules. The interesting result of this section is that the COFs that prevent the β-amyloid aggregation more adequately cross the BBB better; therefore, they can be decent potential options for treating AD.

Coarse-grained (CG) simulation

Figure 7A outlines the results of the coarse-grained simulation. The results show enhanced aggregation of β-amyloid molecules in the absence of any nanostructure. This figure shows that the dispersion of more than 300 amyloid molecules in the presence of amine-functionalized JUC—510—COF is much greater than in the absence of COFs. These very large scales of molecular simulations validate the results obtained from the all-atom simulation. CG simulation also indicates that positively charged JUC—510—COF molecules prevent fibrillation of amyloid molecules. The normalized energy between amyloid and amyloid molecules are shown in Figure 7B. Our scrutinization reveals that the average number of normalized hydrogen bonds in the control group (15) state was higher than in the presence of COF (11), and the number of interactions between amyloids was higher in the control group simulation. This confirms the positive effect of COF nanoparticles. The presence of this nanoparticle has been very effective in reducing intermolecular interactions and creating aggregation instability, *i.e.*, COF compound prevents amyloid fibrillation. This is well illustrated in the secondary structure analysis. Figure 7C shows the presence of COF nanoparticles in creating instability where the presence of COF gives rise to the higher values of bend, turn, and coil structures than those in the absence of COF nano-
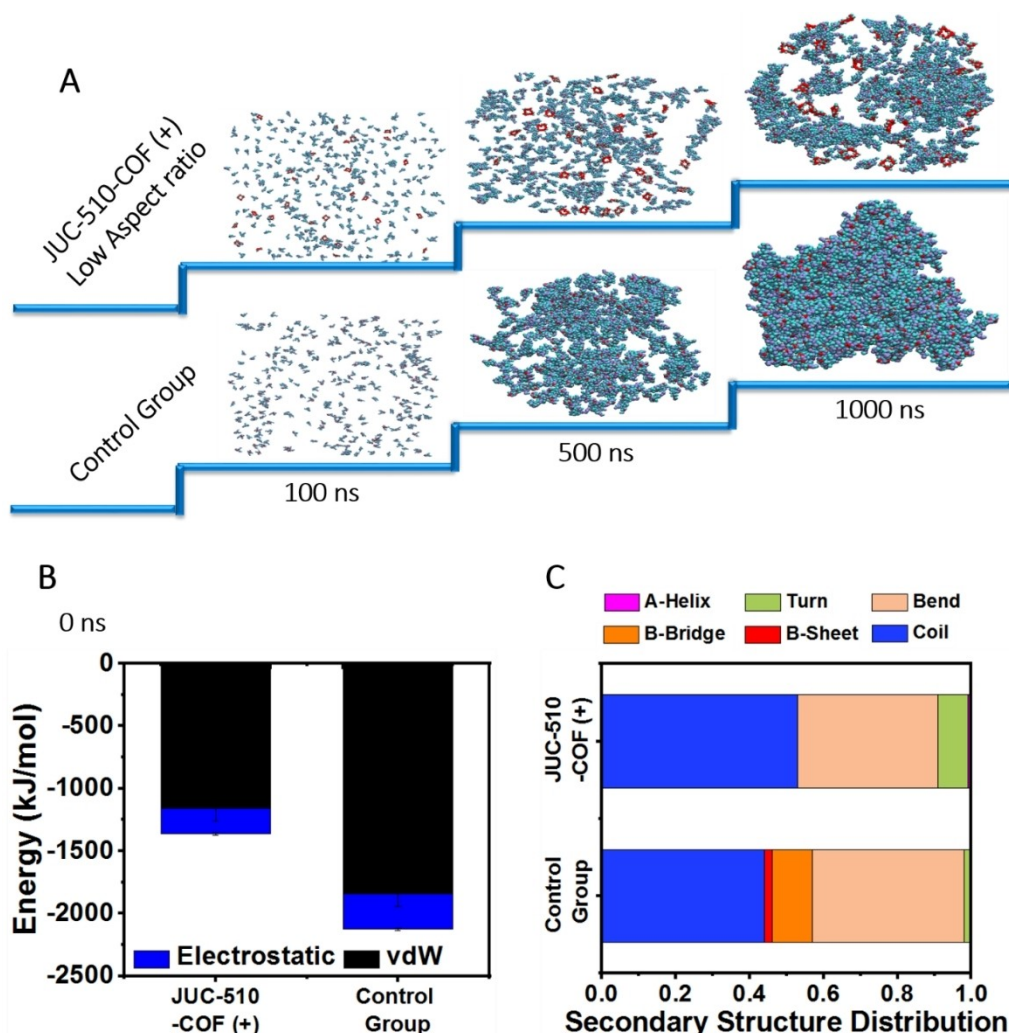
Figure 7. A) Snapshots of the simulation for the control group and in the presence of secondary amine-functionalized JUC—510—COF. The simulations are performed for 1 microsecond. B) energy analysis of amyloid corresponding control group (without COF compound) and in the presence of JUC—510—COF, and C) secondary structure analysis for coarse-grained simulations for the control group and in the presence of secondary amine-functionalized JUC—510—COF.

particles. These three structures cause instability and prevent amyloid fibrillation. In the presence of COFs, the amount of stabilizing parameters also decreases.

Conclusion

In this study, using a multi-scale simulation approach, we have assessed the possible role of COF nano-objects in the inhibition of Aβ aggregation. To the best of our knowledge, the current study is the first to evaluate COF capabilities in this area and we additionally consider the morphological properties of the molecules. Considering the highly tunable feature of COFs, which can be engineered through joint computational and experimental investigations, we selected this new generation of a nanomaterial as a potential candidate for AD treatment. Regarding this matter, we investigated the interaction between six COFs (TPA–COF, CH$_3$–Li-imCOF, Tp–PaSO$_3$Li–COF, COF–OEt, JUC–510–COF, and COF–77) with Aβ to evaluate each COFs ability in inhibiting the fibrillation process behind the AD pathology. After evaluating the secondary structures of Aβ in the presence of COFs, it was observed that the presence of TPA–COF could drop the number of β-sheets to zero and increase the percentage of bends and coils. A decrease in the number of β sheets was also observed in the presence of COF–OEt. However, the existence of Tp–PaSO$_3$Li–COF and especially CH$_3$–Li–ImCOF increased β-sheets structures, which means that these COFs can, in fact, promote β-amyloid aggregation instead of obstructing it. Since a high number of β-sheets is necessary for β-amyloid aggregation, it can be concluded that this particular COF induced conformations in Aβ proteins that are not suitable for β-amyloid aggregations.

Another parameter that contributes to the aggregation process is the contact area. A lower contact area can reduce the probability of β-amyloid aggregation because Aβ/Aβ contact is necessary for the β-amyloid aggregation. The lowest contact area and the highest average number of hydrogen bonds with water were observed in Aβ/JUC–510–COF molecular systems. These results can be associated with the high available surface area of JUC–510–COF due to its aspect ratio. Furthermore, the influence of aspect ratio with a small change in each organic structure was assessed. The obtained results all confirmed our hypothesis proving that nanomaterials with a low aspect ratio (close to one) offer better results regarding β-amyloid inter-action and subsequent self-assembly inhibition. Another important factor is the binding energies (vdW, electrostatic, and their resultant total energy) between COFs and β-amyloid strands, the highest amount of interaction energy is related to the binding energy of the TPA–COF and β-amyloid. With these results in mind, in the third part of this study, another series of simulations were performed with the charged-COFs. As expected and in correlation with previous papers, charged COFs (positively charged followed by negative) have a higher affinity toward β-amyloid monomers. Ultimately, we validated the results using Gibbs free energy calculations to further confirm that positively charged nanomaterials with lower aspect ratios have a higher affinity towards beta amyloids. Taken all together,

JUC–510–COF followed by TPA–COF showed prominent inhibitory effects on the assembly of Aβ monomers. On the contrary, the result of our simulation showed that the presence of Tp–PaSO$_3$Li–COF and CH$_3$–Li–ImCOF could enhance the β-amyloid aggregation and these COFs have limited potential for utilization in Alzheimer's treatment. In another part of our simulation, it was observed that COFs that had an inhibitory effect on β-amyloid aggregation could also prevent β-amyloid fibrilization in and Aβ pentamer protofibrils. Furthermore, the result of the simulation suggested that factors such as hydrophobicity and low aspect ratio contribute to passing through the BBB. Moreover, it was observed positively charged COFs, that result from incorporating an amine group can enhance diffusion through the BBB. It can be deduced from these results that the addition of amine groups not only enhances diffusion through BBB but also can inhibit β-amyloid aggregation. The CG simulations confirmed the findings on a larger scale, confirming once again that the charged COFs can interact with hundreds of β-amyloids and consequently prevents the fibrillation process.

In summary, our results make evident that COFs with variable aspect ratios and geometries have a preference in binding to Aβ protein that can eventually affect their anti-β-amyloidogenic ability. On the other hand, COFs are highly tunable nanoparticles and present a wide variety of structures with diverse morphology that can interact with Aβ protein in different ways. However, whether or not COF molecules can effectively inhibit the self-assembly of the Aβ polypeptide in real-life applications can be considered for future studies *in vitro* and *in vivo*. Our results so far have been very promising and could be a stepping stone for further experimental investigations.

Conflict of Interest

The authors declare no conflict of interest.

Keywords: 2D materials · lzheimer's disease · β-amyloid · covalent organic frameworks · molecular simulation

[1] E. Nichols, C. E. Szoeke, S. E. Vollset, N. Abbasi, F. Abd-Allah, J. Abdela, M. T. E. Aichour, R. O. Akinyemi, F. Alahdab, S. W. Asgedom, *Lancet Neurol.* **2019**, *18*, 88–106.
[2] A. s. Association, *Alzheimer's Dementia* **2018**, *14*, 367–429.
[3] L. Teri, L. E. Gibbons, S. M. McCurry, R. G. Logsdon, D. M. Buchner, W. E. Barlow, W. A. Kukull, A. Z. LaCroix, W. McCormick, E. B. Larson, *JAMA* **2003**, *290*, 2015–2022.
[4] H. A. Fink, E. Jutkowitz, J. R. McCarten, L. S. Hemmy, M. Butler, H. Davila, E. Ratner, C. Calvert, T. R. Barclay, M. Brasure, *Ann. Int. Med.* **2018**, *168*, 39–51.
[5] J. Hardy, D. Allsop, *Trends Pharmacol. Sci.* **1991**, *12*, 383–388.

ChemBioChem

Full Papers
doi.org/10.1002/cbic.202100075

Chemistry Europe
European Chemical
Societies Publishing

[6] R. Liu, H. Barkhordarian, S. Emadi, C. B. Park, M. R. Sierks, *Neurobiol. Dis.* **2005**, *20*, 74–81.

[7] B. Solomon, R. Koppel, E. Hanan, T. Katzav, *Proc. Natl. Acad. Sci. USA* **1996**, *93*, 452–455.

[8] L. Liu, Y. Chang, J. Yu, M. Jiang, N. Xia, *Sens. Actuators B* **2017**, *251*, 359–365.

[9] F. Tahmasebinia, S. Emadi, *BioMetals* **2017**, *30*, 285–293.

[10] G. G. Glenner, C. W. Wong, *Biochem. Biophys. Res. Commun.* **1984**, *120*, 885–890.

[11] J. Kang, H.-G. Lemaire, A. Unterbeck, J. M. Salbaum, C. L. Masters, K.-H. Grzeschik, G. Multhaup, K. Beyreuther, B. Müller-Hill, *Nature* **1987**, *325*, 733–736.

[12] R. J. O'Brien, P. C. Wong, *Ann. Rev. Neurosci.* **2011**, *34*, 185–204.

[13] U. C. Müller, T. Deller, M. Korte, *Nat. Rev. Neurosci.* **2017**, *18*, 281–298.

[14] Y. Zhou, J. S. Richardson, *Neurorep.* **1996**, *7*, 2487–2490.

[15] D. Sul, H.-S. Kim, D. Lee, S. S. Joo, K. W. Hwang, S.-Y. Park, *Life Sci.* **2009**, *84*, 257–262.

[16] G. Tosi, F. Pederzoli, D. Belletti, M. A. Vandelli, F. Forni, J. T. Duskey, B. Ruozi, *Nanomedicine in Alzheimer's Disease: Amyloid-beta Targeting Strategy, Progress in Brain Research*, Elsevier, **2019**, Vol. 245, pp 57–88.

[17] D. Brambilla, R. Verpillot, B. Le Droumaguet, J. Nicolas, M. Taverna, J. Kóna, B. Lettiero, S. H. Hashemi, L. De Kimpe, M. Canovi, *ACS Nano* **2012**, *6*, 5897–5908.

[18] M. Mahmoudi, M. A. Shokrgozar, S. Sardari, M. K. Moghadam, H. Vali, S. Laurent, P. Stroeve, *Nanoscale* **2011**, *3*, 1127–1138.

[19] J. Wu, H. Xie, *Artif. Cells, Nanomed., Biotechnol.* **2016**, *44*, 690–694.

[20] D. Kim, J. M. Yoo, H. Hwang, J. Lee, S. H. Lee, S. P. Yun, M. J. Park, M. Lee, S. Choi, S. H. Kwon, *Nat. Nanotechnol.* **2018**, *13*, 812–818.

[21] K. Debnath, N. Pradhan, B. K. Singh, N. R. Jana, N. R. Jana, *ACS Appl. Mater. Interfaces* **2017**, *9*, 24126–24139.

[22] W.-H. Wu, X. Sun, Y.-P. Yu, J. Hu, L. Zhao, Q. Liu, Y.-F. Zhao, Y.-M. Li, *Biochem. Biophys. Res. Commun.* **2008**, *373*, 315–318.

[23] C. Zhang, X. Wan, X. Zheng, X. Shao, Q. Liu, Q. Zhang, Y. Qian, *Biomaterials* **2014**, *35*, 456–465.

[24] C. Cabaleiro-Lago, F. Quinlan-Pluck, I. Lynch, S. Lindman, A. M. Minogue, E. Thulin, D. M. Walsh, K. A. Dawson, S. Linse, *J. Am. Chem. Soc.* **2008**, *130*, 15437–15443.

[25] S. I. Yoo, M. Yang, J. R. Brender, V. Subramanian, K. Sun, N. E. Joo, S. H. Jeong, A. Ramamoorthy, N. A. Kotov, *Angew. Chem. Intern. Ed.* **2011**, *50*, 5110–5115; *Angew. Chem.* **2011**, *123*, 5216–5115.

[26] E. Araya, I. Olmedo, N. G. Bastus, S. Guerrero, V. F. Puntes, E. Giralt, M. J. Kogan, *Nanoscale Res. Lett.* **2008**, *3*, 435–443.

[27] G. Liu, P. Men, W. Kudo, G. Perry, M. A. Smith, *Neurosci. Lett.* **2009**, *455*, 187–190.

[28] E. Alimohammadi, A. Nikzad, M. Khedri, M. Rezaian, A. M. Jahromi, N. Rezaei, R. Maleki, *Nanomedicine* **2021**, *16*, 189–204.

[29] I. Javed, G. Peng, Y. Xing, T. Yu, M. Zhao, A. Kakinen, A. Faridi, C. L. Parish, F. Ding, T. P. Davis, *Nat. Commun.* **2019**, *10*, 1–14.

[30] K. Giannousi, O. Antonoglou, C. Dendrinou-Samara, *ACS Chem. Neurosci.* **2019**, *10*, 3796–3804.

[31] J. Guo, J. Li, Y. Zhang, X. Jin, H. Liu, X. Yao, *PLoS One* **2013**, *8*, e65579.

[32] C. S. Diercks, O. M. Yaghi, *Science* **2017**, *355*, 6328.

[33] I. Berlanga, Ruiz-M. L. González, González-J. M. Calbet, J. L. G. Fierro, Mas-R. Ballesté, F. Zamora, *Small* **2011**, *7*, 1207–1211.

[34] X. Chen, K. Geng, R. Liu, K. T. Tan, Y. Gong, Z. Li, S. Tao, Q. Jiang, D. Jiang, *Angew. Chem. Intern. Ed.* **2020**, *59*, 5050–5091; *Angew. Chem.* **2020**, *132*, 5086–5091.

[35] S. Bhunia, K. A. Deo, A. K. Gaharwar, *Adv. Funct. Mater.* **2020**, 2002046.

[36] Q. Guan, G.-B. Wang, L.-L. Zhou, W.-Y. Li, Y.-B. Dong, *Nanoscale Adv.* **2020**, *2*, 3656–3733.

[37] H. L. Nguyen, C. Gropp, O. M. Yaghi, *J. Am. Chem. Soc.* **2020**, *142*, 2771–2776.

[38] G. Chedid, A. Yassin, *Nanomater.* **2018**, *8*, 916.

[39] M. C. Scicluna, L. Vella-Zarb, *ACS Appl. Nano Mater.* **2020**, *3*, 3097–3115.

[40] Q. Guan, L. L. Zhou, W. Y. Li, Y. A. Li, Y. B. Dong, *Chem. Eur. J.* **2020**, *26*, 5583–5591.

[41] S. Ciudad, E. Puig, T. Botzanowski, M. Meigooni, A. S. Arango, J. Do, M. Mayzel, M. Bayoumi, S. Chaignepain, G. Maglia, *Nat. Commun.* **2020**, *11*, 1–14.

[42] S. C. Drew, C. J. Noble, C. L. Masters, G. R. Hanson, K. J. Barnham, *J. Am. Chem. Soc.* **2009**, *131*, 1195–1207.

[43] A. Melquiond, G. Boucher, N. Mousseau, P. Derreumaux, *J. Chem. Phys.* **2005**, *122*, 174904.

[44] S. T. Ngo, M. S. Li, *Mol. Simul.* **2013**, *39*, 279–291.

[45] F. Azam, N. H. Alabdullah, H. M. Ehmedat, A. R. Abulifa, I. Taban, S. Upadhyayula, *J. Biomol. Struct. Dyn.* **2018**, *36*, 2099–2117.

[46] J. A. Lemkul, D. R. Bevan, *J. Phys. Chem. B* **2010**, *114*, 1652–1660.

[47] C. Wu, Z. Wang, H. Lei, Y. Duan, M. T. Bowers, J.-E. Shea, *J. Mol. Biol.* **2008**, *384*, 718–729.

[48] M. Song, Y. Sun, Y. Luo, Y. Zhu, Y. Liu, H. Li, *Int. J. Mol. Sci.* **2018**, *19*, 1815.

[49] Y. Zou, Z. Qian, Y. Chen, H. Qian, G. Wei, Q. Zhang, *ACS Chem. Neurosci.* **2019**, *10*, 1585–1594.

[50] T. C. Michaels, A. Šarić, J. Habchi, S. Chia, G. Meisl, M. Vendruscolo, C. M. Dobson, T. P. Knowles, *Ann. Rev. Phys. Chem.* **2018**, *69*, 273–298.

[51] E. B. Walton, K. J. VanVliet, *Phys. Rev. E* **2006**, *74*, 061901.

[52] P. Zandi, E. Ghasemy, A. Khedri, R. Rashidi, R. Maleki, A. Miri Jahromi, *ACS Omega* **2021**, *6*, 6312–6325.

[53] L. Baweja, K. Balamurugan, V. Subramanian, A. Dhawan, *J. Mol. Graphics Modell.* **2015**, *61*, 175–185.

[54] M. Mahdavi, A. Fattahi, E. Tajkhorshid, S. Nouranian, *ACS Appl. Bio. Mater.* **2020**, *3*, 1354–1363.

[55] E. Alimohammadi, M. Khedri, A. M. Jahromi, R. Maleki, M. Rezaian, *Int. J. Nanomed.* **2020**, *15*, 6887.

[56] R. Maleki, M. Khedri, D. Malekahmadi, S. Mohaghegh, A. M. Jahromi, M.-A. Shahbazi, *Mater. Today Commun.* **2021**, *26*, 101948.

[57] Y. Xu, J. Shen, X. Luo, W. Zhu, K. Chen, J. Ma, H. Jiang, *Proc. Natl. Acad. Sci. USA* **2005**, *102*, 5403–5407.

[58] A. Baumketner, *J. Phys. Chem. B* **2014**, *118*, 14578–14589.

[59] Z. Qian, Q. Zhang, Y. Liu, P. Chen, *PLoS One* **2017**, *12*, e0188794.

[60] E. Gazit, *FASEB J.* **2002**, *16*, 77–83.

[61] H. Li, Y. Luo, P. Derreumaux, G. Wei, *Biophys. J.* **2011**, *101*, 2267–2276.

[62] D. Rochu, T. Pernet, F. Renault, C. Bon, P. Masson, *J. Chromatogr. A* **2001**, *910*, 347–357.

[63] G. Pandey, J. Saikia, S. Sasidharan, D. C. Joshi, S. Thota, H. B. Nemade, N. Chaudhary, V. Ramakrishnan, *Sci. Rep.* **2017**, *7*, 1–9.

[64] J. Saikia, G. Pandey, S. Sasidharan, F. Antony, H. B. Nemade, S. Kumar, N. Chaudhary, V. Ramakrishnan, *ACS Chem. Neurosci.* **2019**, *10*, 2250–2262.

[65] N. Zhang, X. Hu, P. Guan, K. Zeng, Y. Cheng, *J. Phys. Chem. C* **2018**, *123*, 897–906.

[66] Y. H. Liao, Y. J. Chang, Y. Yoshiike, Y. C. Chang, Y. R. Chen, *Small* **2012**, *8*, 3631–3639.

[67] H. Mohammad-Beigi, A. Hosseini, M. Adeli, M. R. Ejtehadi, G. Christiansen, C. Sahin, Z. Tu, M. Tavakol, A. Dilmaghani-Marand, I. Nabipour, *ACS Nano* **2019**, *13*, 3243–3256.

[68] H. Qosa, B. S. Abuasal, I. A. Romero, B. Weksler, P.-O. Couraud, J. N. Keller, A. Kaddoumi, *Neuropharmacol.* **2014**, *79*, 668–678.

[69] B. Shackleton, C. Ringland, L. Abdullah, M. Mullan, F. Crawford, C. Bachmeier, *Mol. Neurobiol.* **2019**, *56*, 8296–8305.

[70] Y.-J. Wang, H.-D. Zhou, X.-F. Zhou, *Drug Discovery Today* **2006**, *11*, 931–938.

[71] R. Dal Magro, S. Simonelli, A. Cox, B. Formicola, R. Corti, V. Cassina, L. Nardo, F. Mantegazza, D. Salerno, G. Grasso, *Front. Neurosci.* **2019**, *13*, 419.

[72] H. Qosa, Y. S. Batarseh, M. M. Mohyeldin, K. A. El Sayed, J. N. Keller, A. Kaddoumi, *ACS Chem. Neurosci.* **2015**, *6*, 1849–1859.